

## Article

# Transformations in Flow Characteristics and Fluid Force Reduction with Respect to the Vegetation Type and Its Installation Position Downstream of an Embankment

A H M Rashedunnabi <sup>1</sup>, Norio Tanaka <sup>2,3,\*</sup> and Md Abedur Rahman <sup>4</sup>

<sup>1</sup> Department of Mathematics, Faculty of Science, University of Rajshahi, Rajshahi 6205, Bangladesh; rashed\_math@ru.ac.bd

<sup>2</sup> Graduate School of Science and Engineering, Saitama University, Saitama 338-8570, Japan

<sup>3</sup> Department of Resilient Society, Research Center for Social Transformation, Saitama University, Saitama 338-8570, Japan

<sup>4</sup> Tokyo Civil Engineering Branch, Maeda Corporation, Tokyo 102-0072, Japan; shobuj059@gmail.com

\* Correspondence: tanaka01@mail.saitama-u.ac.jp

**Abstract:** Compound mitigation systems, integrations of natural and engineering structures against the high inundating current from tsunamis or storm surges, have garnered significant interest among researchers, especially following the Tohoku earthquake and tsunami in 2011. Understanding the complex flow phenomena is essential for the resilience of the mitigation structures and effective energy reduction. This study conducted a flume experiment to clarify flow characteristics and fluid force dissipation in a compound defense system. Vegetation models (V) with different porosities ( $\Phi$ ) were placed at three different positions downstream of an embankment model (E). A single-layer emergent vegetation model was considered, and a short-layer vegetation with several values of  $\Phi$  was incorporated to increase its density (decreased  $\Phi$ ). Depending on  $\Phi$  and the spacing (S) between the E and V, hydraulic jumps occurred in the physical system. The findings demonstrated that a rise in S allowed a hydraulic jump to develop inside the system and contributed to reducing the fluid force in front and downstream of V. Due to the reduced porosity of the double-layer vegetation, the hydraulic jump moved upstream and terminated within the system, resulting in a uniform water surface upstream of V and downstream of the system. As a result, the fluid force in front of and behind V reduced remarkably.

**Keywords:** tsunami overtopping; compound mitigation system; vegetation porosity; hydraulic jump; fluid force



Academic Editors: Jaan H. Pu, D. Andrew S. Rees, Manish Pandey, Prashanth Reddy Hanmaiahgari and Bimlesh Kumar

Received: 17 October 2024

Revised: 10 January 2025

Accepted: 14 January 2025

Published: 17 January 2025

**Citation:** Rashedunnabi, A.H.M.; Tanaka, N.; Rahman, M.A.

Transformations in Flow Characteristics and Fluid Force Reduction with Respect to the Vegetation Type and Its Installation Position Downstream of an Embankment. *Fluids* **2025**, *10*, 16. <https://doi.org/10.3390/fluids10010016>

**Copyright:** © 2025 by the authors. Licensee MDPI, Basel, Switzerland. This article is an open access article distributed under the terms and conditions of the Creative Commons Attribution (CC BY) license (<https://creativecommons.org/licenses/by/4.0/>).

## 1. Introduction

The catastrophic 2011 Tohoku Earthquake and tsunami caused an enormous loss of lives and loss to the economy in the northeast coastal community of Japan. The Ministry of Land, Infrastructure, Transport, and Tourism of Japan classified this catastrophic occurrence as a Level 2 tsunami because it would recur in several hundred to a thousand years [1]. The inundation depth reached approximately 10 to 40 m, overwhelming the coastal defense structures, which led to the destruction of parts of these structures and widespread flooding of inland areas [2]. Tsunami walls, coastal dykes, and tsunami gates collapsed, and coastal forests were destroyed [3,4]. The consequences were severe, including a significant number of deaths, huge property and building destruction, and a substantial impact on the economy. The destructions were severe where the structural defense was partially or totally

collapsed [3,5]. The post-tsunami survey revealed that some of the coastal dykes, especially those with forests behind them, were able to survive the impact of the tsunami waves [6].

Tsunami mitigation strategies since the 2011 disaster have indeed evolved from relying on single approaches to adopting multiple and hybrid defense systems. This shift is driven by the recognition that no single structural method can completely protect against the diverse and complex nature of a tsunami wave. Hybridizations combining ecosystem-based approaches such as coastal or mangrove forests, coral reefs, dunes, and structural defenses like tsunami-break waters, seawalls, and large embankments perform better than single measures [4,7,8]. The use of land is also a high priority in the coastal mitigation strategies. Multiple-layer defense systems comprising structural approaches such as coastal dikes, seawalls, and embankments with a buffer zone of a coastal forest were proposed for a future tsunami mitigation strategy in Japan, and a pilot project is continuing [9].

However, extensive research is required to elucidate the mechanisms of multiple mitigation systems against the impact of tsunami currents and is necessary prior to implementation. The recent studies on compound defense strategies in coastal areas have highlighted the effectiveness of integrating natural and engineered structures against environmental hazards such as tsunamis or storm surges. These strategies combined different elements to create a better mitigation method, which includes a coastal forest and moat [10], an embankment with trees followed by another embankment [11], a dune and canal [12], an embankment moat and forest [13], a double-layer forest behind a coastal embankment [14], or a canal behind an embankment [15].

Recent studies have shown that combining an embankment with a backward-facing, vertically double-layered forest can generate a water cushion by forming a hydraulic jump between the structures, which helps to reduce the downstream overflow energy [14,16]. The flows can easily pass through the vegetation and sometimes form a hydraulic jump inside or close to the vegetation due to the higher porosity of the vegetation. In contrast, vegetation with higher resistance (due to lower porosity) can induce a submerged hydraulic jump on the downward-facing slope of the embankment, which may prevent embankment erosion [14]. Additionally, when the overflow depths are increased, the hydraulic jump might not develop within the available space of the hybrid defense system and can extend into the vegetation, resulting in strong undulations and passing through the vegetation. Strong roller vortices in the counterclockwise direction have been observed during the jump as flow moves from left to right; these vortices produce scour holes [17].

A recent flume study conducted on a movable bed explored the scouring phenomenon in a compound defense system comprising a double-layer of vegetation and an embankment. The study revealed that the double-layer vegetation could reduce scouring up to a maximum of about 34%. However, the scour length covered around 64% of the space between the embankment and vegetation, and, in some cases, the scour hole reached the vegetation model. It was recommended that the gap between the embankment and coastal forest should be adjusted to reduce scouring at the embankment toe and achieve optimal performance from such a compound defense system [16].

Therefore, in order to achieve optimal mitigation effects against destructive tsunami forces and ensure the sustainability of the mitigation structures, it is necessary to understand how the position and length of the hydraulic jump are affected by changes in the distance between the vegetation and embankment. Additionally, fluid force should be reduced to minimize damage from the breakage and washing out of trees and houses in the inland [18].

In recent years, most studies on compound or hybrid mitigation systems have concentrated primarily on the flow characteristics and scouring phenomena between the structures and have estimated the total energy reduction by the defense system [14,16,19]. Some recent studies have examined the energy heads behind the single-layer emergent vegetation in

compound structures [13,20]. However, they did not address the fluid force downstream that results from these kinds of compound defense systems when double-layer vegetation is implemented.

Therefore, this study aimed to find an optimal compound mitigation method comprising a seaside embankment and a landward double-layer forest. Considering the highest overflow from the embankment, single-layer and double-layer vegetation of different porosities were used, varying the length of the open space ( $S$ ) between the embankment and the vegetation. To explore the effectiveness, a flume experiment was conducted in which the installation position of the vegetation was varied to understand the complex flow phenomena within the mitigation system and its effect on the fluid force on the vegetation and downstream the mitigation system.

The objectives of this study were as follows:

- Assess the impact of vegetation porosity on the flow characteristics and scouring phenomena within the mitigation system;
- Determine the optimal length of the open space between the embankment and vegetation to minimize scouring and enhance the stability of the embankment;
- Evaluate the formation and position of hydraulic jumps relative to different configurations of the mitigation system;
- Investigate the downstream fluid force and its potential to cause damage to inland structures, aiming to reduce such forces effectively.

For these objectives, the flume experiment involved varying the position and porosity of the vegetation while monitoring the flow patterns and the behavior of hydraulic jumps. The findings from this investigation are expected to provide insights into the optimal configuration of a compound defense system that maximizes the mitigation of destructive tsunami forces and ensures the sustainability of the mitigation structures.

## 2. Materials and Methods

### 2.1. Features of Experimental Flume and Flow Conditions

An experimental flume at the Hydraulic and Environmental Engineering Lab of Saitama University was used for the experiments. The flume dimensions were 15 m long, 0.7 m high, and 0.5 m wide. A pump was installed at the start of the flume to ensure continuous water circulation, regulated by a measurement software called “Hydra 2.0”, which maintains a constant discharge rate ( $\text{m}^3/\text{s}$ ). A gently descending slope with a gradient of 1/200 was designed to achieve supercritical flow conditions. Achieving a Froude number ( $Fr$ ) greater than 1, ( $Fr = \bar{v}/(gh)^{0.5}$ , where  $h$  stands for the water depth (m),  $\bar{v}$  denotes the depth-averaged velocity (m/s), and  $g$  is the acceleration ( $\text{m}/\text{s}^2$ ) due to gravity, is essential to simulate the high-velocity, turbulent conditions that characterize tsunami currents [21,22]. For this experiment, a comprehensive range of five  $Fr$  numbers (1.38, 1.44, 1.49, 1.52 and 1.56) was selected. These values ensure that the embankment and vegetation models placed on the flume bed will face higher forces, providing insights into their robustness under extreme conditions.

A visualization of the experimental setup is depicted in Figure 1a. To evaluate the flow phenomena with respect to the  $Fr$  numbers, five critical overtopping flow depths ( $h_c$ ) were selected: 0.030 m, 0.038 m, 0.055 m, 0.069 m, and 0.04 m.

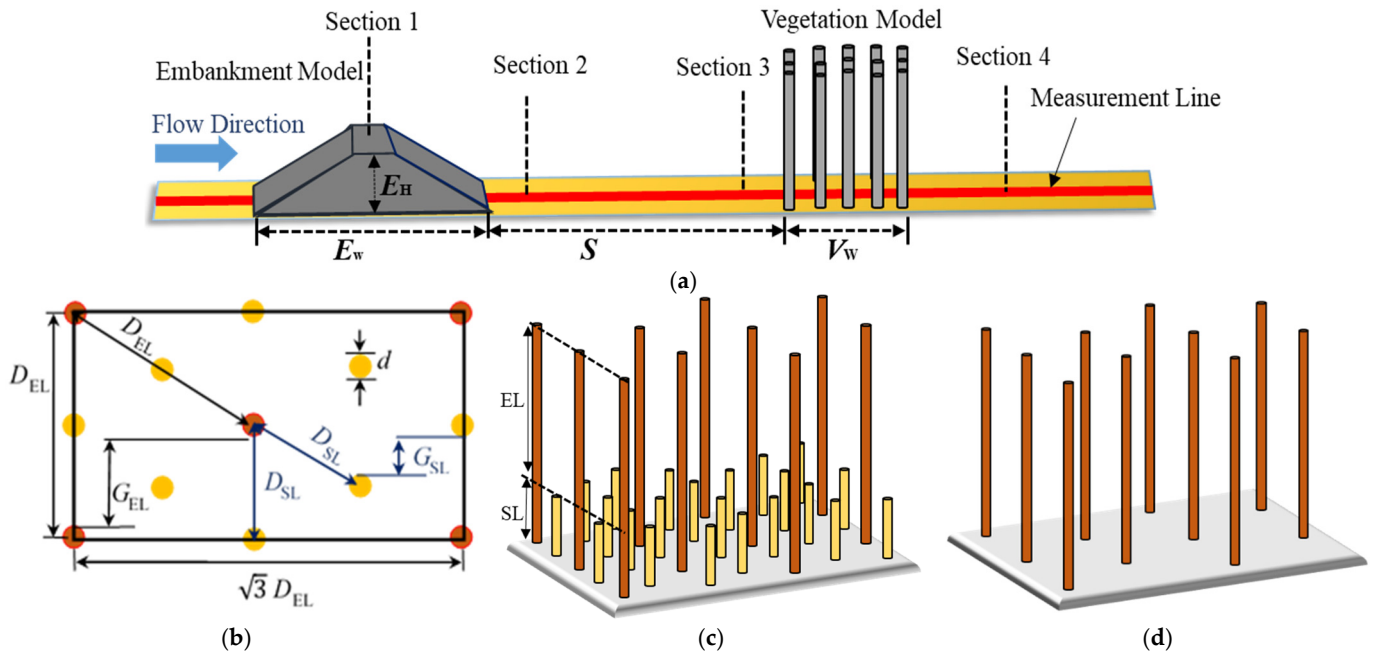


**Figure 1.** Experimental setup: (a) flume with experimental models, (b) vegetation arrangement; red and yellow color dots represent the tall and short vegetation respectively, (c) double-layer vegetation model, and (d) single-layer emergent vegetation where  $E_H$  and  $E_W$  are the embankment height and width, respectively,  $S$  is the open space between the embankment and vegetation,  $V_W$  is the width of the vegetation,  $D_{SL}$  and  $D_{EL}$  are the center-to-center distance between the cylinders in the submerged layer (SL) and emergent layer (EL), respectively, and  $G_{SL}$  and  $G_{EL}$  are the gap between the trees in the SL and EL, respectively, the two sided arrows represent the distance or heights.

2.2. Compound Mitigation Models

In this experimental setup, a compound mitigation system was designed to simulate the mechanisms of coastal protection. The system comprised a seaward embankment (E) and a vegetation model (V) containing both single and double-layer vegetation configurations, SV and DV, respectively. A 1:100 scale physical model was selected to replicate the real conditions on a reduced scale. The E model was built with wooden planks with a height of 14.5 cm and an inclination of 1:2, which was constructed using an actual scenario [9]. Circular wooden cylinders were chosen for their simplicity and ease of construction, with specific diameters (0.04 m) to mimic the emergent and submerged layers of coastal vegetation. The trees of the emerged (EL) and submerged (SL) layers of V were simulated by wooden cylinders with a diameter ( $d$ ) of 0.004 m and heights of 0.18 m and 0.05 m, respectively [23] (Figure 1b–d). In this study, the following formula was derived to evaluate the integrated porosity  $\Phi_I$  of the vegetation models.

$$\Phi_I = 1 - \frac{\pi d^2 (n_{t1} h_1 + n_{t2} h_2)}{4\sqrt{3} D^2 h} \tag{1}$$

where  $h_1$  and  $h_2$  denote the relative heights of SL and EL, and  $n_{t1}$  and  $n_{t2}$  are the number of trees in each layer, respectively,  $h = h_1 + h_2$ , and  $D$  is the center-to-center distance between the emergent cylinders in the transverse direction of flow (Figure 1b). Table 1 shows the experimental cases where the number in the subscript of V means the vegetation porosity.

**Table 1.** Experimental cases.

Experimental Cases	$h'_c$	$D_{EL}$ (cm)	$D_{SL}$ (cm)	$G_{EL}$ (cm)	$G_{SL}$ (cm)	$\Phi_I$ (%)
EN	0.21, 0.26, 0.38, 0.47, 0.51	--	--	--	--	--
ESV <sub>98</sub>	0.21, 0.26, 0.38, 0.47, 0.51	2.5	--	0.85	--	98
EDV <sub>88</sub>	0.21, 0.26, 0.38, 0.47, 0.51	2.5	1.25	0.85	0.225	88
EDV <sub>83</sub>	0.21, 0.26, 0.38, 0.47, 0.51	2.5	1.25	0.85	0.225	83
EDV <sub>70</sub>	0.21, 0.26, 0.38, 0.47, 0.51	2.5	0.833	0.85	0.0167	70

Note: EN: embankment only (no vegetation); ESV: embankment and single-layer emergent vegetation; and EDV: embankment and double-layer (submerged with emergent) vegetation, where the subscripts of V stand for the respective vegetation's porosity  $\Phi_I$  (%).  $h'_c = h_c/E_H$ ;  $h_c$  is the critical water depth defined in Figure 2; and  $H_E$ ,  $D_{EL}$ ,  $D_{SL}$ ,  $G_{EL}$ , and  $G_{SL}$  are defined in Figure 1, the -- means the parameter is not used.

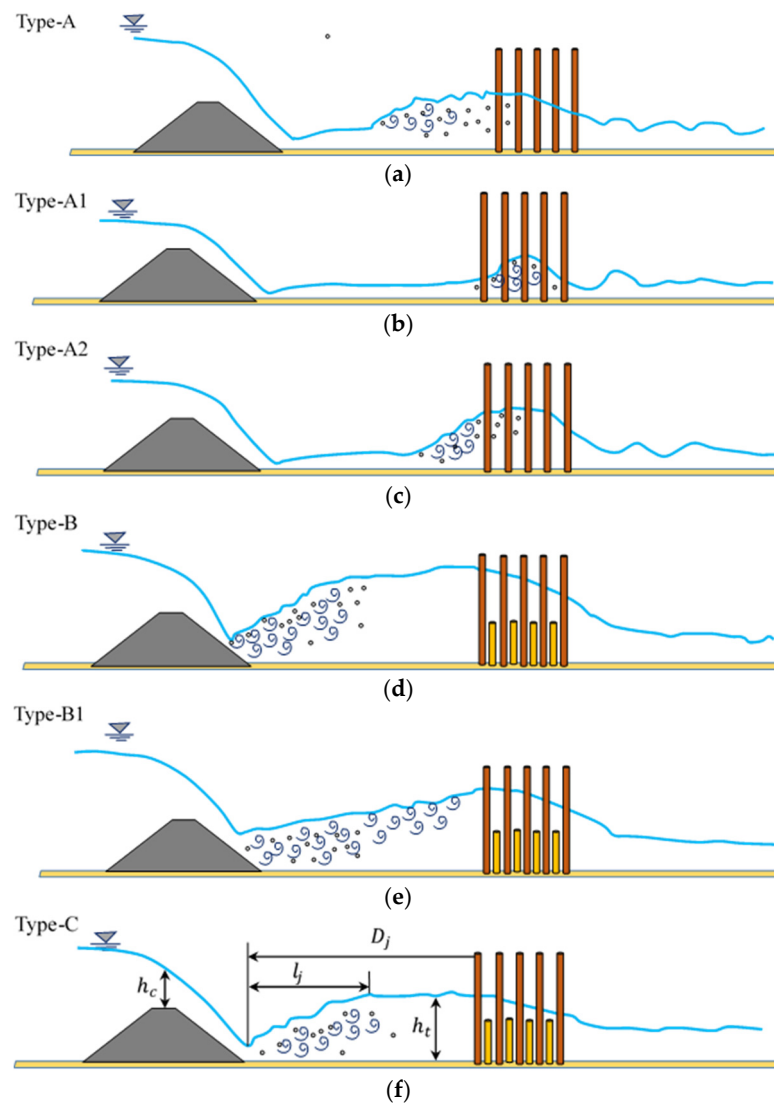


**Figure 2.** Sketch of flow structure in the experimental scenario: (a), Type-A, (b) Type-A1, (c) Type-A2, (d) Type-B, (e) Type-B1, and (f) Type-C, where the jump types represented in (a–c) occur for Case ESV and (d–f) occur for Case EDV, the dots and spiral symbols represents the eddies generated in the jump.

### 2.3. Collecting and Analyzing Data

#### 2.3.1. Water Surface Profile and Velocity Measurement

Once the E and individual V models were installed in the experimental setup, the chosen flows were consistently maintained. The water level was recorded at the middle of the flume in order to accurately record the effect of vegetation on the flow. Depending on the variations in the water surface levels, these measurements were made at regular intervals between 1 and 5 cm. This interval range ensured a detailed and precise understanding of the variations in water depth induced by the presence of vegetation.

The flow velocity in the mitigation system was measured using a particle image velocimetry (PIV) instrument (Green Laser Sheet 200 m/G, Kato Koken Co., Ltd., Kanagawa, Japan). The measurements were taken at two specific locations: 5 cm upstream of the vegetation and 7 cm downstream of the vegetation. This arrangement allowed a detailed analysis of the flow dynamics and the effects of the vegetation on the flow velocity in the channel.

#### 2.3.2. Fluid Force Estimation

The flow in the composite defense system becomes very complex, and, sometimes, the oscillations approach or pass through the vegetation because hydraulic jumps are formed [14,24]. Since the hydraulic jumps are expected to occur within the open space  $S$ ,  $V$  can be affected by the strong flow force generated due to overtopping E. The dynamic fluid force is a crucial parameter in fluid dynamics and is essential for understanding and designing various engineering systems. In particular, the vegetation behind a dam must consider the dynamic forces exerted by flowing water to ensure the sustainability of such counter measures. Therefore, in this study, the dynamic fluid force ( $F_D = \rho v^2/2$ ,  $\rho$  is the density of water ( $\text{kg}/\text{m}^3$ ), and  $v$  is the velocity measured in front of the vegetation in Section 3 (Figure 1a)) was estimated to explore the effects of the complex flow on V.

In addition, the fluid force is a crucial factor in the breaking or washing away of structures or trees downstream of the mitigation system. To determine the breakage and washout conditions of trees and houses, the fluid force ( $F$ ) acting on these structures can be calculated using the following equation [18]:

$$F = \frac{1}{2} C_d \rho d_{\text{BH}} F I \quad (2)$$

where  $C_d$  and  $d_{\text{BH}}$  represent the coefficient of drag and characteristic diameter of a tree at breast height, respectively,  $\rho$  is the density of the water, and  $FI = \bar{v}^2 h$ ,  $\bar{v}$  is the depth-averaged flow velocity, and  $h$  is the water depth. The fluid force index ( $FI$ ) was utilized as a key factor to determine the conditions for breakage and the washout of trees or structures. This parameter was estimated in Section 4 (Figure 1a) to evaluate the impact of V downstream the mitigation system.

In this study, the flow forces were estimated in front of and behind the forest for all experimental cases. These estimates help to understand the susceptibility of the vegetation to breakage and washout conditions downstream under different flow conditions and vegetation scenarios.

### 2.4. Non-Dimensional Parameters

The following important dimensionless parameters were considered to analyze the flow characteristics in the mitigation system:

$$f_1(Fr, h'_c, \phi_I, D'_j, L'_j, h'_t, S'_i, F'_D, \Delta FI) = 0 \quad (3)$$

where  $h'_c = h_c/H_E$  ( $h_c$  is the critical depth,  $H_E$  is the embankment height),  $D'_j = D_j/S_i$  ( $D_j$  is the hydraulic jump distance from the vegetation front, and  $S_i$  ( $i = 1, 2, 3$ ) is the spacing between E and V;  $S_1 = 0.5$  m,  $S_2 = 1$  m, and  $S_3 = 2.5$  m),  $h'_t = h_t/h$  ( $h_t$  is the tail-water depth of the hydraulic jump (in Section 3), and  $h$  is the height of V),  $S'_I = S_i/W_v$  ( $W_v = 0.2427$  m is the vegetation width),  $F'_D = F_{DV}/F_{DN}$  ( $F_{DV}$  is the dynamic fluid force after the placement of V, and  $F_{DN}$  is the dynamic fluid force without V (only E) at Section 3 (Figure 1a)), and  $\Delta FI = (FI_{EN} - FI_{EV})/FI_{EN}$  ( $F_{EN}$  is the fluid force index in Case EN, and  $F_{EV}$  is the fluid force index in E and V cases (Figure 1)).

### 3. Results

#### 3.1. Transformation of the Flow in the Mitigation System

Several types of flow structures have been differentiated in the defense system, especially in the vegetation and the embankment models. A gradually varied flow structure was observed for the embankment-only case. In contrast, the flow turned into a hydraulic jump when confronted with vegetation downstream. The position of the jump varied depending on  $\Phi_I$  and  $S'$  values. The types of hydraulic jumps varied according to their position of origin in a horizontal or near-horizontal bed facing a steep upstream slope. A Type-A jump is defined when its initial position is on the horizontal bed, and Type-B is defined when the jump occurs on the steep upstream slope and continues on the downstream slope. Type-C is defined when the jump location is at the contact or transition point, and, if it occurs entirely on the upstream slope, it is defined as Type-D [25–28].

Three different kinds of hydraulic jumps were identified in this investigation: Type-A, Type-B, and Type-C, based on their location on the flume bed and embankment slope (Figure 2). In addition, three distinct jump variations were observed in this experiment, which were initiated but remained undeveloped or incomplete within the mitigation system. As the jump type greatly affects the dynamic component of the fluid force on V and behind the compound structure, these jumps are classified as Type-A1, A2 and B1 (Figure 2). Type-A1 is defined when the jump position is inside the vegetation, Type-A2 means the jump starts on the flume bed (in front of V) but does not finish within the  $S$ , and Type-B1 indicates that the jump starts on the embankment slope but the jump does not finish within  $S$ .

Figure 3 shows the location of the hydraulic jump and its classification using  $h'_c$  and  $\Phi_I$ , where the legends  $ESV_{xx}-S_i$  and  $EDV_{xx}-S_i$  in Figure 3a mean the experimental cases with vegetation porosity and spacing for  $xx$  and  $S_i$ , respectively. On the other hand, a gradually varied flow was observed downstream of the system, and there were no significant changes in the flow with respect to  $S_i$  and  $\Phi_I$ . Figure 4 represents some real hydraulic jumps in the experimental cases. These are discussed in the next sections.

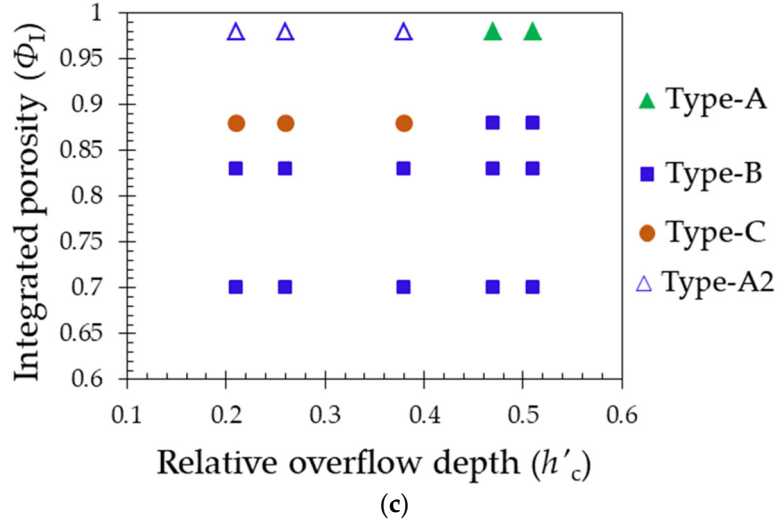
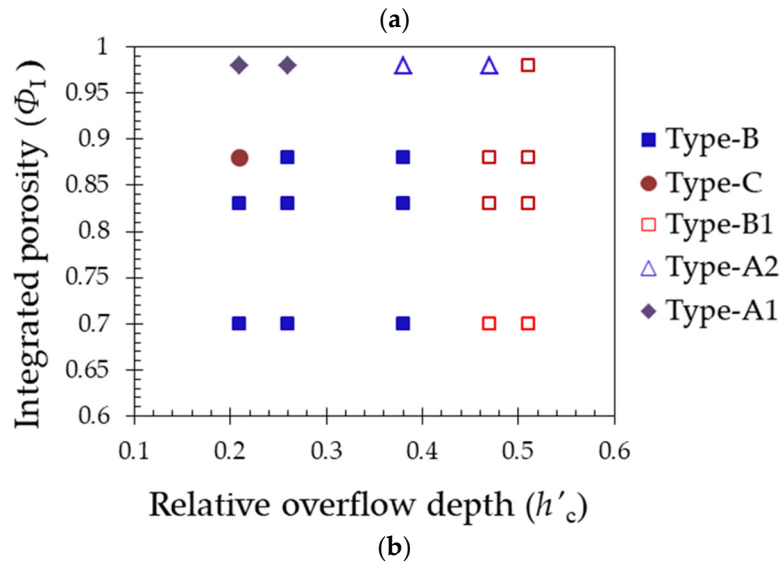
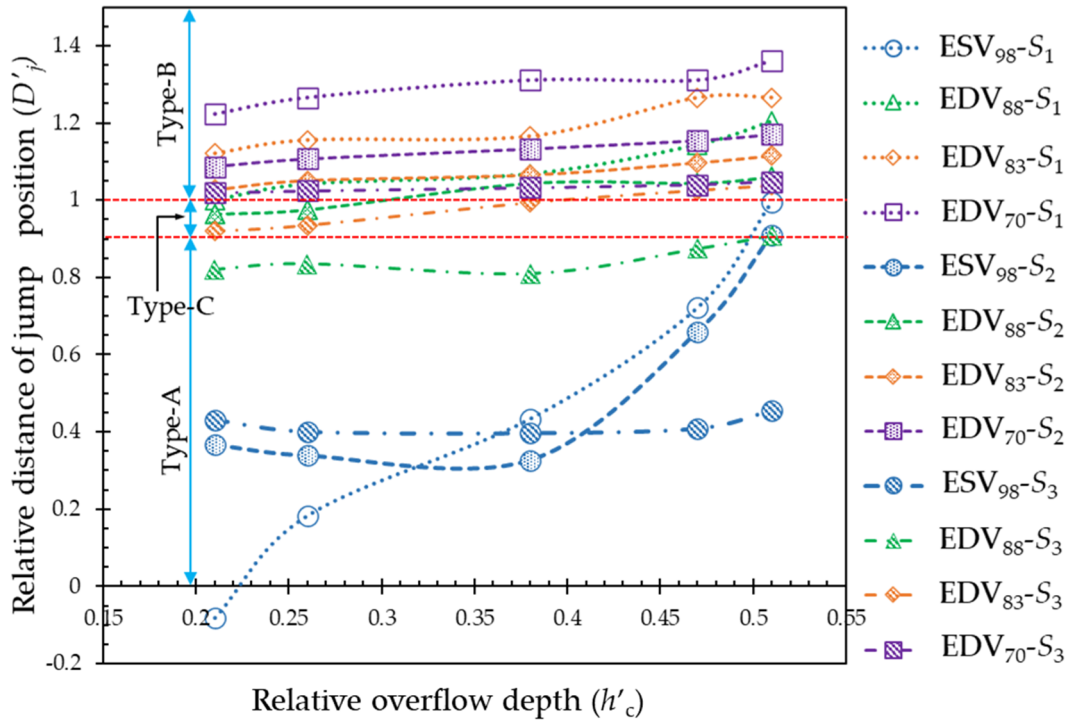


Figure 3. Cont.

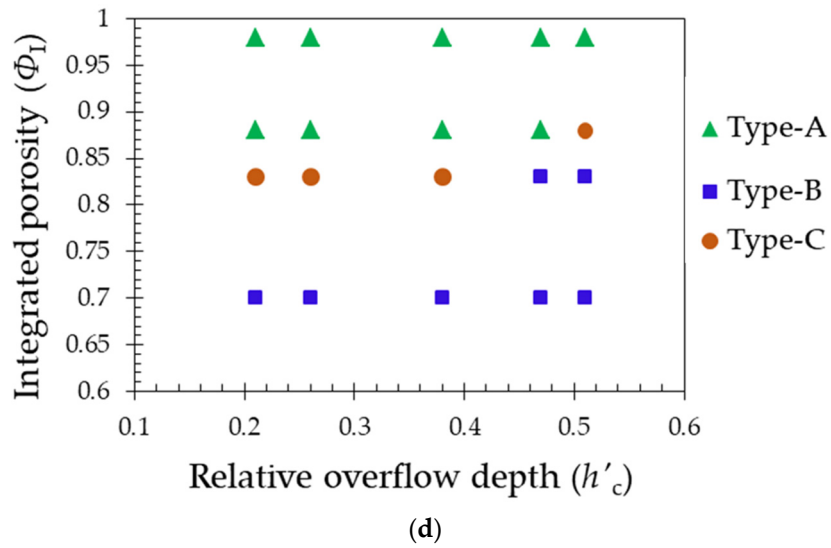


Figure 3. Hydraulic jump classification: (a) relative jump position and flow type for (b)  $S_1$ , (c)  $S_2$ , and (d)  $S_3$ , the red dotted lines are the boundaries of Type-C.

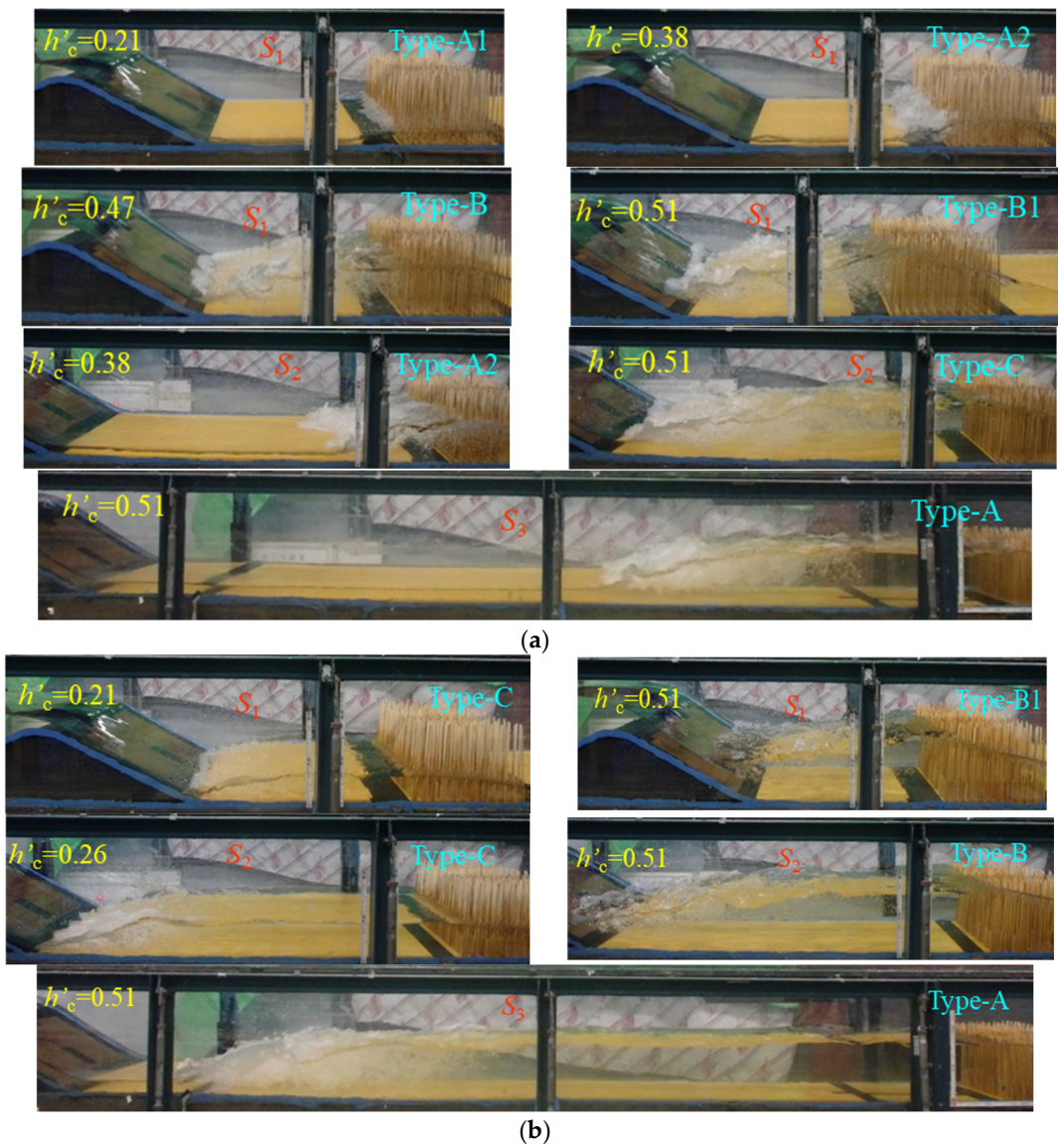
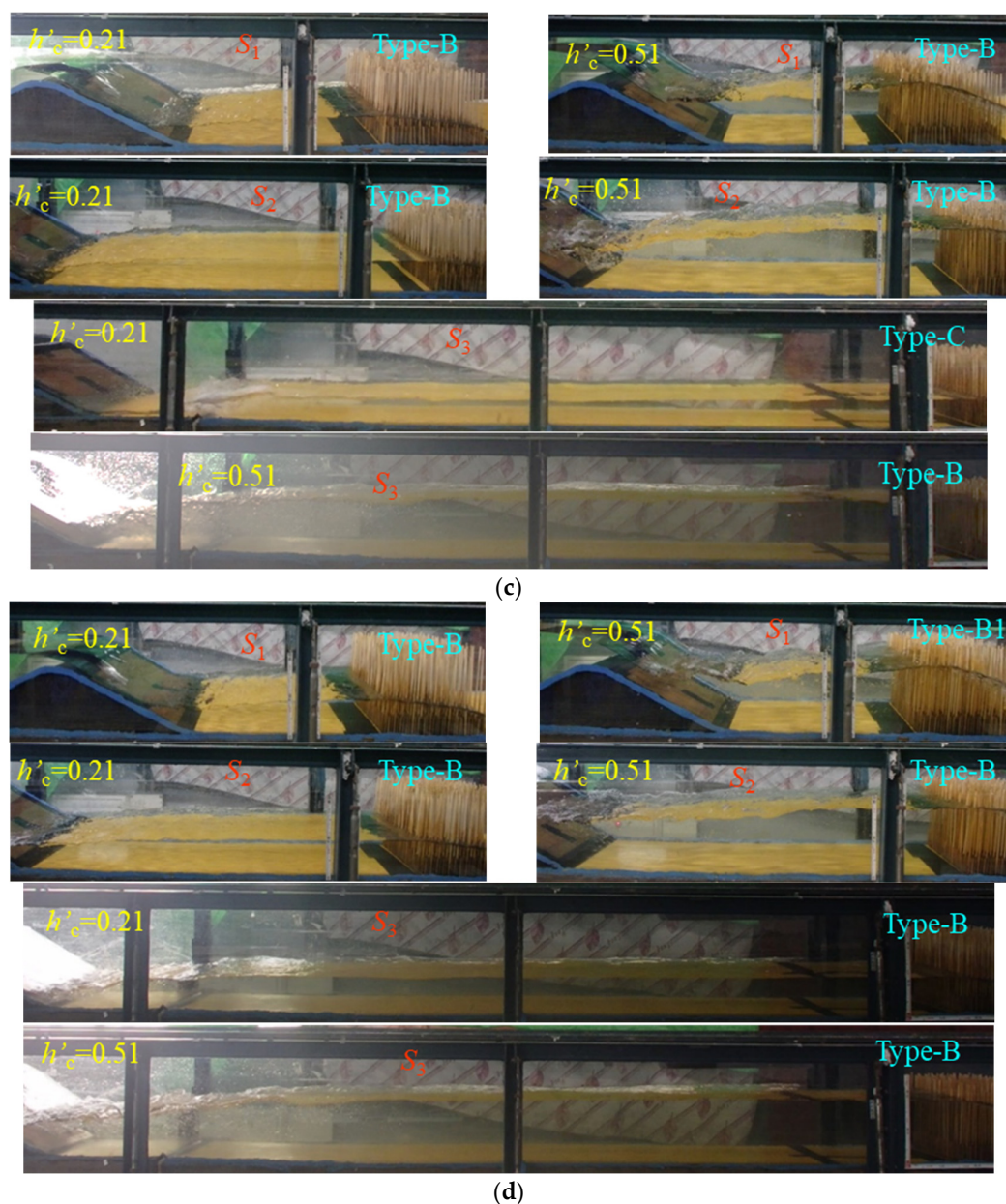


Figure 4. Cont.



**Figure 4.** Flow structures in the experimental flume: (a) Case ESV<sub>98</sub>, (b) Case EDV<sub>88</sub>, (c) Case EDV<sub>83</sub>, and (d) Case EDV<sub>70</sub>.

### 3.2. Changes in Hydraulic Jump Properties

#### 3.2.1. Relative Position of Jump and Jump Type

The hydraulic jump positions in relation to the flow circumstances for all of the experimental cases are presented in Figure 3. Jump types are classified with respect to the value of the relative distance of the jump position  $D'_j$  ( $=D_j/S_i$ ) from the vegetation model to upstream. Type-A, Type-B, and Type-C are classified according to the values  $D'_j < 0.9$ ,  $D'_j > 1$ , and  $0.9 < D'_j < 1$ , respectively, whereas  $D'_j < 0$  indicates that the jump starts inside the vegetation, not within the space between the vegetation and the embankment model. The value of  $D'_j$  changes with changing the  $h'_c$ ,  $S'_I$ , and  $\Phi_I$ , respectively. Figure 3b–d show the flow type changes with respect to  $\Phi_I$  and  $S'_i$ . Figure 4 shows some real photographs of the flow types in the experimental scenario.

For the experimental Case ESV<sub>98</sub> with the minimum spacing  $S'_1$ , a hydraulic jump was initiated inside the vegetation, and the jump position moved upstream but did not develop in the range of  $h'_c$  from 0.21 to 0.47 (Figures 3a and 4a). Only Type-C was observed

for the highest value 0.51 of  $h'_c$  (Figures 3a and 4a). However, the position of jump moved upward the vegetation for  $S'_2$  and  $S'_3$ . Only the Type-A jump was observed for this case. The jump was fully developed when the spacing was maximum ( $S'_3$ ) in this experiment (Figure 3d).

The hydraulic jump changed from Type-C to Type-B for Case EDV<sub>88</sub> in the experimental flow range for  $S'_1$  and  $S'_2$  (Figure 3b,c and Figure 4b). The Type-B1 jump was observed only for the highest value of  $h'_c$  with the minimum spacing (Figure 3c). But there was no Type-B jump while the spacing was maximum ( $S'_3$ ). In addition, the Type-A jump was formed for  $0.21 \leq h'_c \leq 0.47$ , and only Type-C was observed for  $h'_c = 5.1$  (Figure 3d).

Only a Type-B jump was formed for Case EDV<sub>83</sub> against all of the flow conditions for both of  $S'_1$  and  $S'_2$  (Figure 3b,c). Type-B1 was created for  $h'_c = 0.47$  to 0.51 with the minimum spacing ( $S'_1$ ) (Figure 4b). When the spacing was increased to  $S'_3$ , the jump type transformed to Type-C for  $0.21 \leq h'_c \leq 0.38$ , while Type-B remained unchanged  $h'_c > 0.38$  (Figures 3d and 4c).

On the other hand, a Type-B jump was always formed for Case EDV<sub>70</sub> for all  $h'_c$  and  $S'_i$  (Figures 3b–d and 4d). Type-B1 was observed for the highest flow range 0.47–0.51 when the spacing was minimum ( $S'_1$ ) (Figure 3d).

### 3.2.2. Relative Hydraulic Jump Length and Tail-Water Depth

Figure 5a shows the ratio of the hydraulic jump length ( $L_j$ ) to the open space ( $S$ ) and the tail-water depth ( $h_t$ ) to the vegetation height ( $H_v$ ) in this investigation. The parameters were considered when a jump was fully developed in between the E and V models. A hydraulic jump was not formed and/or developed within the open space  $S$  in some experimental cases, especially in Case ESV<sub>98</sub>. On the contrary, the jump length fully covered the open space and was not developed fully in Case EDV<sub>83</sub> and EDV<sub>70</sub> for  $h'_c = 0.47, 0.51$  and in Case EDV<sub>88</sub> for  $h'_c = 0.51$  with the minimum spacing  $S'_1$ . The parameters are not displayed in the figure in such cases.

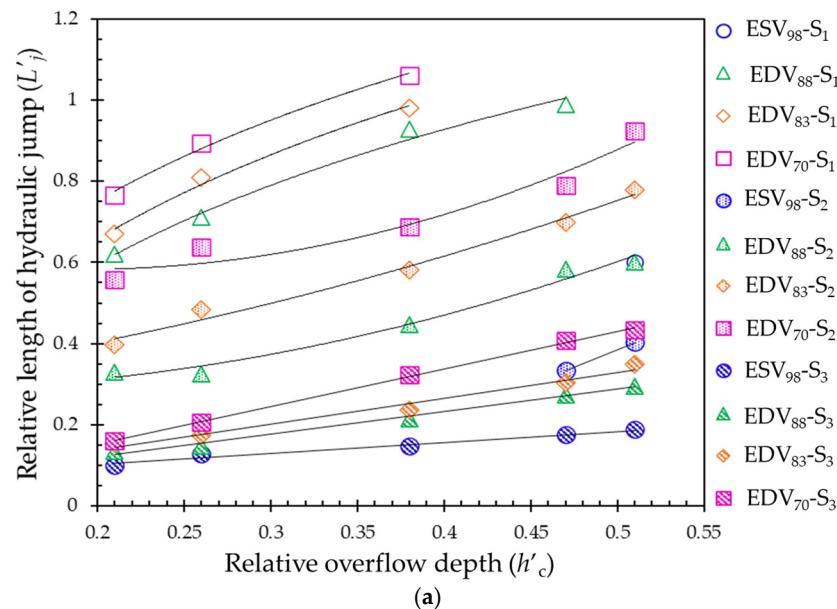
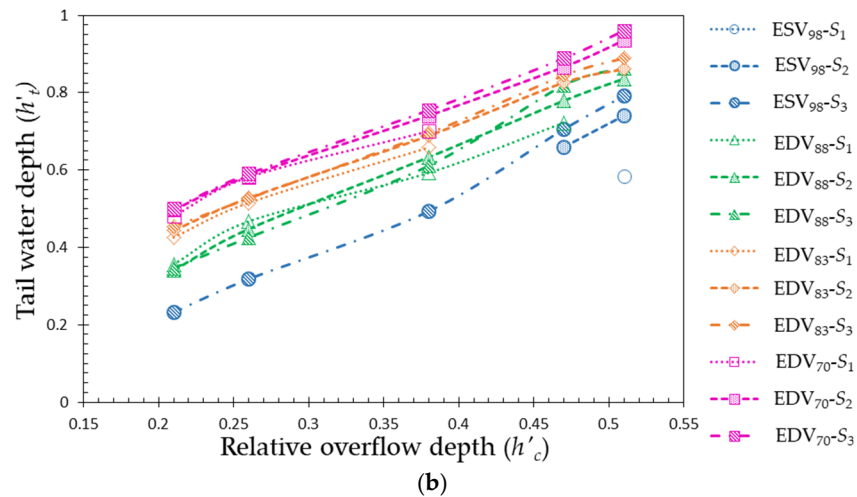


Figure 5. Cont.



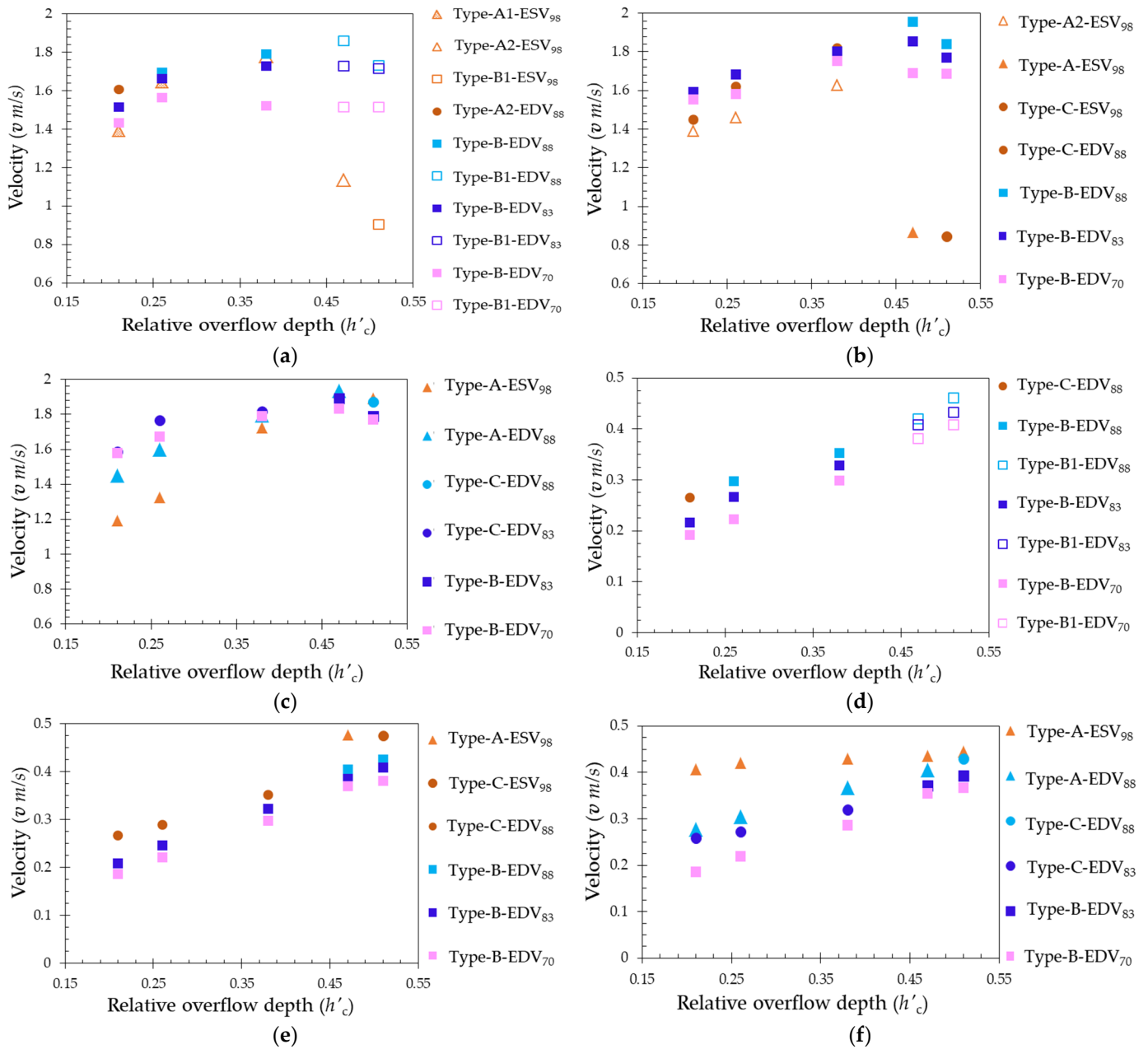
**Figure 5.** Hydraulic jump parameters: (a) hydraulic jump length (with trend), and (b) relative tail-water depth.

Figure 5a shows that  $L'_j$  increases with increasing  $h'_c$  and decreasing  $\Phi_1$ . The maximum  $L'_j$  was observed in Case EDV<sub>70</sub> and the minimum in Case ESV<sub>98</sub> for each value of  $S'_i$ . The graph shows that the parameter value decreases with the increasing value of  $S'_i$  in a specific case. The changing trends of the parameter are also clear in Figure 5a. It was increased logarithmically, exponentially, and linearly for  $S'_1$ ,  $S'_2$ , and  $S'_3$ , respectively, while the jump length covered around 15–40% of the open space. The trend was exponential when the jump length covered around 35–80%, and it became logarithmic when the length of that  $S$  covered started from 60%.

The tail-water depth in front of the vegetation model was measured when the hydraulic jump was fully developed within the open space between the vegetation and embankment. The relative tail-water depth  $h'_t$  observed in this experiment is displayed in Figure 5b. The graph shows that  $h'_t$  increased almost linearly with increasing  $h'_c$  and  $S'_i$  in Case EDV<sub>83</sub> and EDV<sub>70</sub>. The maximum value of  $h'_t$  was observed in Case EDV<sub>70</sub> for  $S'_3$ . Increasing the value of  $S'_i$  increased  $h'_t$  2–8% with respect to a flow condition in a specific case. It was also observed that the relative tail-water depth varies according to the type of the jump. For a fixed value of  $h'_c$ , the value of  $h'_t$  was increasing with increasing  $S'_i$  when the jump remained Type-B. On the other hand,  $h'_t$  was decreasing with increasing  $S'_i$  in Case EDV<sub>88</sub> when the jump was either Type-C or Type-A or transformed from Type-B to Type-C or from Type-C to Type-A. The minimum value of  $h'_t$  was in Case ESV<sub>98</sub> in this experiment.

### 3.2.3. Velocity Upstream and Downstream of Hydraulic Jump

It is observed from Figure 6a–c that the velocity before the hydraulic jump is the minimum in Case ESV<sub>98</sub> compared to the other cases, which varied between 0.85 and 1.25 m/s. On the other hand, the values change from 0.33 to 0.42 m/s, which was found to be the maximum in the downstream of a hydraulic jump in comparison to other experimental cases. The velocity in the double-layer vegetation cases varied from 1.42 to 1.93 m/s in the upstream, while it was between 0.18 and 0.47 m/s in the downstream of the hydraulic jump. The  $v$  grew both upstream and downstream of the hydraulic jump as the  $h'_c$  increased. Figure 6 shows that the  $v$  in the upstream grew as the jump changed its type from A to C and later to B. In contrast, as its type changed in the same sequence, it declined downstream of the jump. Type-B had the lowest velocity downstream of the jump. It is observed that  $v$  decreased as the open distance between the E and V increased.



**Figure 6.** Velocity: (a)  $S_1$ , (b)  $S_2$ , (c)  $S_3$  in the upstream and (d)  $S_1$ , (e)  $S_2$ , and (f)  $S_3$  in the downstream (at Section 3 in Figure 1a) of the hydraulic jump.

### 3.3. Dynamic Fluid Force in Front of Vegetation

The dynamic fluid force ( $F_D$ ) was estimated in Section 3 (Figure 1a) to understand the impact of  $V$  on fluid force. The tail-water depth in this section is sufficient when the hydraulic jump was far ahead of  $V$ , and this parameter was estimated only for these cases. The parameter values were not considered when the jump position was within or very close to  $V$ . The non-dimensional dynamic fluid force  $F'_D$  for individual  $V$  models is represented in Figure 7.

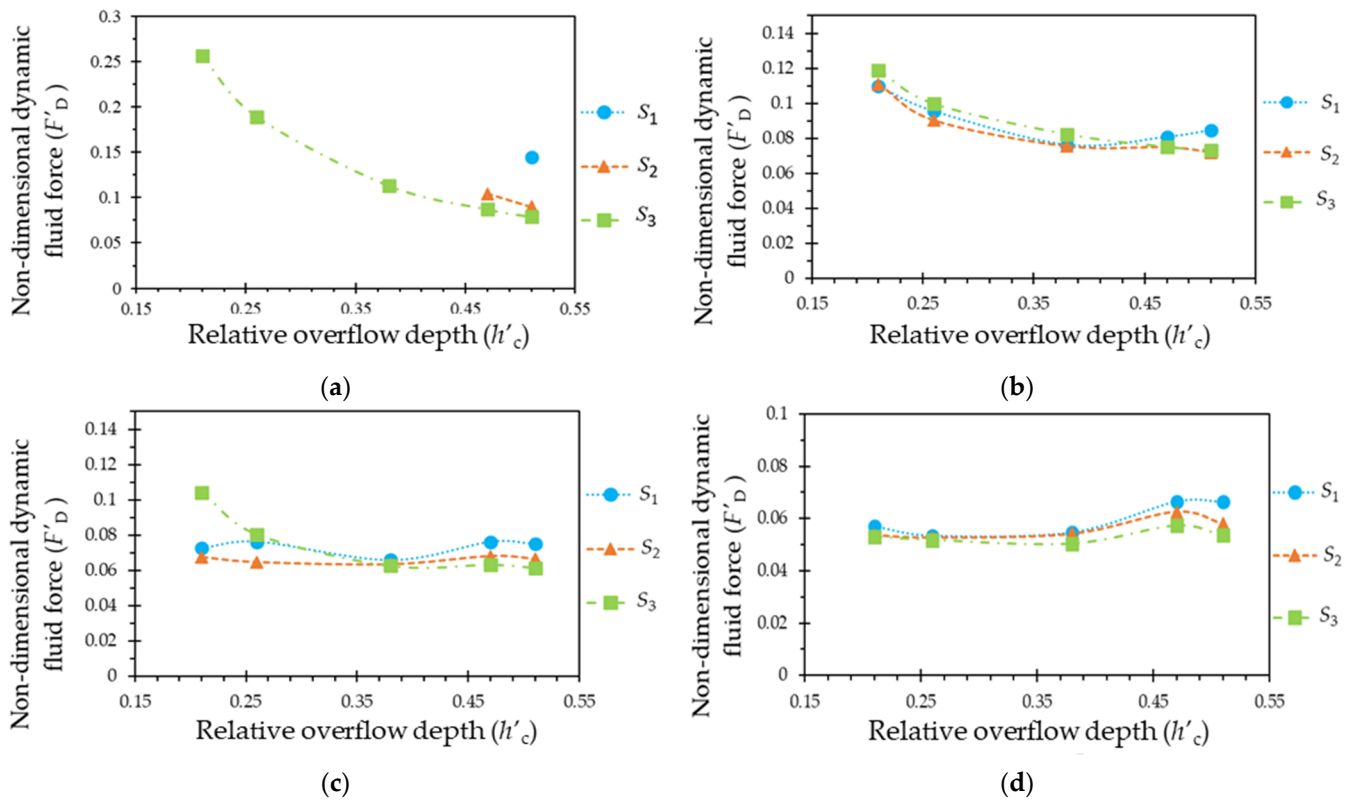


**Figure 7.** Dynamic fluid force in front of vegetation: (a) Case ESV<sub>98</sub>, (b) Case EDV<sub>88</sub>, (c) Case EDV<sub>83</sub> and (d) Case EDV<sub>70</sub>.

It can be observed that the  $F'_D$  value in Case ESV<sub>98</sub> decreased with increasing  $h'_c$ . The trend was exponential for  $S'_3$ . The parameter value was higher for  $S'_1$  and  $S'_2$  than  $S'_3$ . The highest value was about 0.25 for  $S'_3$ . It was about 0.15 for  $S'_1$  with the highest value of  $h'_c = 0.51$ .  $F'_D$  decreased slightly with increasing  $h'_c$  for  $S'_1$ ,  $S'_2$ , and  $S'_3$  in Case EDV<sub>83</sub>.  $F'_D$  also slightly increased with the increasing value of  $S'$  for  $h'_c < 0.48$  and decreased slightly for  $h'_c \geq 0.48$ . The maximum value was 0.12 for  $S'_3$  with a minimum of  $h'_c (=0.21)$ , and the minimum value was reached at 0.072 for  $S'_2$  with the highest value of  $h'_c (=0.51)$ . In Case EDV<sub>83</sub>,  $F'_D$  was almost constant for all values of  $h'_c$  with  $S'_2$ , at about 0.067. For  $S'_1$  and  $S'_3$ , however, both increasing and decreasing trends were observed. For  $S'_3$ , it was about 0.1 and 0.61 with  $h'_c = 0.21$  and  $h'_c = 0.51$ , respectively. In this experimental case, the higher value of  $F'_D$  was observed for the higher range of  $h'_c (>0.38)$  with  $S'_1$ . It is evident that, in Case EDV<sub>70</sub>, the  $F'_D$  value was considerably lower. For all cases of  $S'$ , the value was less than 0.06 and remained almost steady until  $h'_c = 0.38$ . As  $h'_c$  grew,  $F'_D$  showed a little increase for  $S'_1$  and a reduction for  $S'_2$  and  $S'_3$ . The highest  $F'_D$  was approximately 0.66 for  $S'_1$  with  $h'_c = 0.51$ .

### 3.4. Fluid Force Index Downstream of Vegetation

The depth-averaged velocity ( $\bar{u}$ ) was used to calculate the fluid force index ( $FI$ ) behind the vegetation (Section 4 in Figure 1a). Figure 8 shows the reduction in the  $FI$  compared to the case where only the embankment was implemented for each cases with respect to  $S'_i$ . The graph shows that the relative reduction rate  $\Delta FI$  (%) increased with increasing  $h'_c$  for each vegetation model. For a given value of  $h'_c$ , the parameter value decreased slightly with increasing  $S'_i$  in Cases ESV<sub>98</sub> and EDV<sub>88</sub>. On the other hand, Case EDV<sub>83</sub> showed both an increasing and decreasing trend for a fixed value of  $h'_c$ , whereas the percentage of reduction in  $\Delta FI$  increased with increasing  $h'_c$  and  $S'$  in Case EDV<sub>70</sub>. The greatest reduction

was almost 35% at  $h'_c = 0.51$  for  $S'_1$ , and the minimum was 5% against  $h'_c = 0.21$  for  $S'_3$  in Case  $ESV_{98}$ .

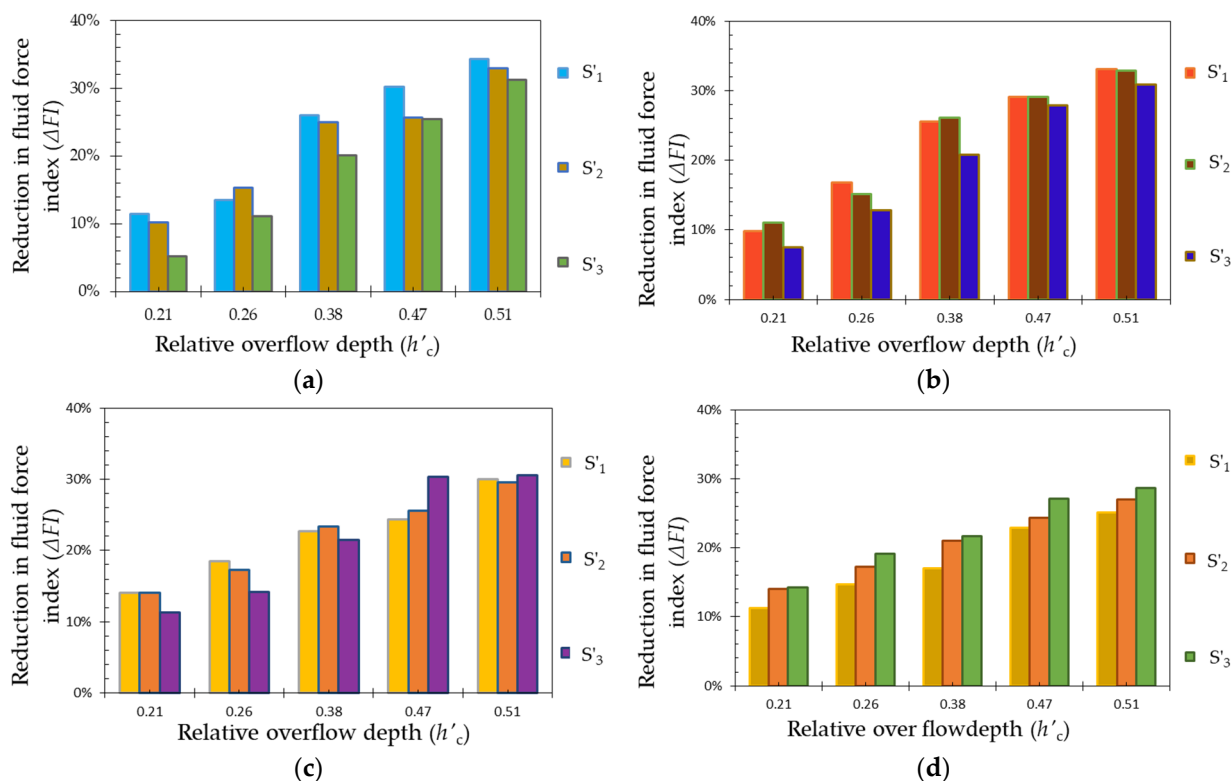


**Figure 8.** Total loss in fluid force index behind vegetation (at Section 3): (a) Case  $ESV_{98}$ , (b) Case  $EDV_{88}$ , (c) Case  $EDV_{83}$ , and (d) Case  $EDV_{70}$ .

Figure 8b shows the reduction in  $\Delta FI$  (%) in Case  $EDV_{88}$ . The data show that the parameter value changed slightly with the change in the  $S'_i$  value. The reduction was almost the same for  $S'_1$  and  $S'_2$  with respect to the  $h'_c$  values. On the other hand, the reduction was decreased when it was increased to  $S'_3$ . The reduced value of  $\Delta FI$  varied between 7% and 33% depending on  $h'_c$  and  $S'_i$ . It is observed that the relative reduction rate of  $\Delta FI$  is almost constant in the range of 0.38–0.51 of the  $h'_c$  value regardless of the  $S'_i$  value in Case  $EDV_{83}$ . However, for the smaller values 0.21 and 0.26 of  $h'_c$ , the reduction rate decreased by 1–4% with increasing  $S'_i$  values (Figure 8c).

On the other hand, the reduction rate of  $\Delta FI$  in Case  $EDV_{70}$  was slightly increased with the increase in  $h'_c$  and  $S'_i$  values (Figure 8d). The minimum reduction rate was about 11% for  $h'_c = 0.21$  and  $S'_1$ , and the maximum value was about 29% for  $h'_c = 0.51$  and  $S'_3$ .

The results show that the percentage reduction in  $\Delta FI$  varied with the hydraulic jump type. The quantity was decreased when the jump type transformed from Type-B > Type-C > Type-A, and the amount was reduced. It was slightly increased or remained almost similar with respect to the  $h'_c$  and  $S'_i$  values when the jump type remained unchanged. The observed range of variation in the reduction percentage was highest in Case  $ESV_{98}$  and lowest in Case  $EDV_{70}$ .

### 4. Discussion

#### 4.1. Flow Characteristics

The 2011 tsunami revealed the limits of existing tsunami mitigation structures due to their massive destruction. To reduce the devastation caused by future tsunamis, a plan to build multilayer tsunami protection utilizing a combination of seawalls, forests,

elevated roadways, and existing highways has been proposed for Sendai City, Japan, the most severely damaged area from the 2011 tsunami effect [29]. Since several structures are intended to be integrated for future mitigation, it is crucial to take into account both the defense system's complex flow structures and sustainability as well as their capacity to reduce the impact of tsunamis. This work clarified the flow characteristics of a compound mitigation system consisting of an E and a V. The flow structure in such a system and its effect on the V and downstream conditions were clarified by testing the vegetation at three locations behind the embankment against different overtopping flow depths.

Flow structures are very complex in multiple defense systems. When an obstruction was placed downward of a steeply descending slope, the water level in the structures rose, resulting in a hydraulic jump [25,30]. When the flow overtopped the embankment in this experiment, it faced a steep downslope and vegetation on a nearly horizontal slope. There were several kinds of hydraulic jumps made in the open area between the E and the V. Similar to earlier research, this study classified jumps based on where they occurred within a complex system with a variable slope [14,25,30]. In a vegetated flume with supercritical flow conditions, hydraulic jumps occurred, and the jump location shifted upstream of the vegetation as its density and thickness increased [31]. In a multifaceted channel with a sharp upward gradient, the jump toe shifted onto the steep slope due to the rise in tail-water depth, and the type of the jump switched from A to B [32]. In this experiment, when the emergent vegetation of a fixed density and width was installed behind the E, the flow structures did not change noticeably. But when a submerged layer with varying porosities was incorporated in the emergent vegetation, there were remarkable changes. As the submerged layer's porosity decreased, the hydraulic jump position moved upward. The changes in flow characteristics in this experiment are discussed below.

The results showed no appreciable changes in the flow structure in the open space  $S'_1$  in Case ESV<sub>98</sub>, and the high energy overtopping flow easily passed through the vegetation when  $h'_c < 0.38$ . It was then placed in front of the vegetation, facing the range of overflow depths  $0.38 \leq h'_c \leq 0.47$ , to form Type-A2 and the highest overflow depth  $h'_c = 0.51$  to form Type-B2 jumps (Figure 3b). Because the vegetation was stiff, the water depth inside the V rose with rising  $h'_c$ , the interaction with the flow stream increased, and the jump position shifted upstream (Type-A1 jump). But with a fixed  $h'_c$ , the extent of open space rose to  $S'_2$ , and the flow changed from a Type-B1 to a Type-C jump. When this value was increased further to  $S'_3$ , the jump type stabilized, and Type-A was formed and completely developed despite all flow circumstances (Figure 3d). When the jump type was A2 or B2, as in Case ESV<sub>98</sub>, there was significant undulation up to the vegetation, making it impossible to quantify the flow characteristics in these situations. The hydraulic jump covered around 20% of the  $S$  when the jump type was A and about 30% of the  $S$  when the jump type was C (Figure 5a). Additionally, the Type-A jump has a greater relative tail-water depth in front of the vegetation than the Type-C jump. As a result, when the V was positioned with the maximum gap of  $S'_3$ , the flow stabilized following the jump (Figure 4a).

In contrast to Case ESV<sub>98</sub>, the porosity of V in Case EDV<sub>88</sub> dropped due to a submerged layer that created a greater flow resistance. As a result, the water surface rose, and a hydraulic jump was formed within the open space  $S$ . For  $S'_1$  and  $h'_c > 0.38$ , the hydraulic jump only started but did not complete within the available space. As for  $S'_2$  and  $S'_3$ , the jump evolved against all values of  $h'_c$  and changed into Type-A and Type-C. About 98% and 60% of the maximal hydraulic jump length ( $L'_j$ ) were covered in  $S_1$  and  $S_2$ , respectively (Figure 5a). On the other hand, the maximum value was found to be 29% in  $S_3$ . In this experimental situation, increasing the  $S'$  value had little effect on the  $h'_t$  value; instead, it grew by roughly 1–10%. The  $L'_j$  value was discovered to be a determining factor, and the findings indicated that lowering the  $L'_j$  raised  $h'_t$ .

In Case EDV<sub>83</sub>, decreasing the porosity of V resulted in a greater rise in water level within the space S, shifting the jump location further upstream in comparison to Cases ESV<sub>98</sub> and EDV<sub>88</sub>. In the lower range of  $h'_c$  ( $=0.21$  to  $0.38$ ), only Type-C was identified for  $S'_3$ , and the jump was Type-B for  $S'_1$ ,  $S'_2$ , and  $S'_3$  (Figure 3). In the greater range of  $h'_c$ , the maximum jump length was the length of S, approximately 98%, 78%, and 34% for  $S_1$ ,  $S_2$ , and  $S_3$ , respectively, and the minimum was 67%, 39%, and 15% for  $S_1$ ,  $S_2$ , and  $S_3$  correspondingly against the minimum of  $h'_c$  (Figure 5a). The  $h'_t$  ranged from 1% to 5% against all of values of  $h'_c$ , regardless of the  $S'$  value. It was discovered to be independent of  $h'_c$  but not  $L'_j$ .

In contrast, Case EDV<sub>70</sub> shows that the jump type is independent of  $h'_c$  and  $S'$ . However, as  $S'$  grew,  $L'_j$  shrank by about 60%, and the  $h'_t$  value climbed by around 2% to 6%. It is thus observed that, by making V less porous, the water depth in the open area between E and V rose, moving the jump position upstream and establishing a submerged hydraulic jump. The relative length of the hydraulic jump diminished as the distance between E and V expanded for a specified porosity of V. Moving the position of V further downstream yields additional water depth in front of the vegetation and calms and steadies the water surface, even though the percentage gain is not very large.

It was found that the velocities upstream and downstream of a hydraulic jump also depend on the position of the hydraulic jump. In the experimental cases, the jump position varied from inside the vegetation to the slope of the embankment, which influenced the velocity. In a Type-A jump, the jump position was on the flume bed, and, thus, the velocity was observed to be lower compared to the other types. It was increased in the Type-C and B jumps because the jump position moved further upstream. In contrast, while the Type-B jump formed and the jump become stabilized, the tail-water depth increased, and the  $v$  was observed to be reduced in front of the vegetation, which occurred in the double-layer vegetation with minimum porosity and maximum open space. In the single-layer vegetation, the tail-water depth declined, and, thus, the velocity in front of the vegetation increased compared to the double-layer cases of V. It is evident that increasing  $s'$  values reduced  $v$  in front of V.

The devastation in 2011 was extreme, with the tsunami walls and embankments completely or partially destroyed. Due to the coastal forest behind it, some of the coastal dykes survived. According to recent studies [5,33], the water was deeper in front of the forest, and a submerged hydraulic jump was formed around the levees, which prevented the levees from eroding. There was significant undulation along the hydraulic jump's length, which is thought to have caused the scouring that extended up to the vegetation front with the maximum overtopping flow and within the 50 cm gap between the embankment and vegetation [19,34]. In light of the dikes' overall stability, the National Institute for Land and Infrastructure Management suggested and/or put into practice shielding the dikes' slope and topping them with thick concrete blocks and strengthening the leeward toe's soil to prevent scouring [9]. It follows that, in order to lessen the erosion caused by the impact of high intensity wave flows around V and the toe of E, a Type-B jump must be formed, and its length must be reduced. In this experiment, Case EDV<sub>70</sub> with  $S'_3$  fulfills both demands. Therefore, raising S was found to be useful for stabilizing the hydraulic jump in cases where the porosity of V is very low.

#### 4.2. Mitigating Fluid Forces

Any surface or item in touch with a fluid can be affected by the dynamic force of the fluid. The dynamic pressures imposed by moving water must be taken into consideration while building hydraulic structures, such as spillways and dams, or soft measures, like vegetation, to ensure structural integrity. The water depth increased in front of the vegeta-

tion when a super-critical flow encountered resistance from it, turning the flow subcritical and creating a hydraulic jump upstream of the vegetation [14,20,31,35]. Water rises in front of the vegetation and changes the hydraulic jump length, and the surface undulation that results after the jump depends on the vegetation's density and flow condition [14,20,24]. This experiment also revealed that  $\Phi_1$  and  $S_1$  affected the parameters  $L_j$ ,  $h_t$  and  $v$  (Figure 5a,b and Figure 6). Some of the coastal vegetation was washed out and broken during the 2011 tsunami, which resulted in additional damage to areas downstream [9,33,36]. Thus, both structural sustainability and lowering the force of tsunamis on the coastal environment should be prioritized. To comprehend the effect of a complicated flow on  $V$  and the force exerted in the downstream environment, this study assessed this parameter in front of  $V$  and the fluid force index behind  $V$ .

The dynamic fluid force in the compound mitigation system was compared with the fluid force in Case EN. The purpose of this comparison is to better understand how the vegetation is affected by the overtopping flow's dynamic force. Flow overtopping the embankment resulted in a very high fluid force downstream; however, when  $V$  was implemented, the fluid force decreased (Figure 6). Figure 6a illustrates that the  $F'_D$  was extremely high for values of  $h'_c$  and decreased with higher values of  $h'_c$  when the  $V$  of 98%  $\Phi_1$  was applied behind the E. It can be observed in Figure 7a that, when the  $V$  of 98%  $\Phi_1$  was applied behind the E, the  $F'_D$  decreased with rising  $h'_c$  and was extremely high for smaller values of  $h'_c$ . As  $h'_c$  increased, the hydraulic jump's position shifted upward, as shown in Figure 3a, which indicates that it was quite near to the  $V$  for small values of  $h'_c$ . The  $F'_D$  was thus found to be highly dependent on the jump position. However, as  $S'$  was increased, the jump position moved upward from the  $V$ , and  $v$  decreased with a minimum range of  $h'_c$ . As a result,  $F'_D$  is likewise decreased.

The jump position in Case EDV<sub>88</sub> was nearly at the embankment toe (Figure 3a), and it increased as  $h'_c$  increased. Little difference was found when the  $S'$  value was changed, and it was noticed that the  $F'_D$  was reduced slightly due to increasing  $v$  with an increase in  $h'_c$ . For  $h'_c = 0.48$  and  $0.51$  with  $S'_1$ , the  $F'_D$  was found to be 14% higher than the value with  $S'_2$  and  $S'_3$ . Strong undulation was seen, and the jump length persisted up to  $V$ , which slightly increased the  $v$  in front of  $V$  when the open space value was at its lowest ( $S'_1$ ). This had an impact on the  $F'_D$  value.

$F'_D$  was discovered to be nearly constant against the  $h'_c$  in Case EDV<sub>83</sub> with  $S'_1$  and  $S'_2$ . With smaller values of  $h'_c$  with  $S'_3$ , the parameter value was found to be 35–40% higher. It is evident that, in this instance, the hydraulic jump location moved from the embankment down slope to the flume bed, which contributed to reducing the velocity increase in the  $F'_D$  value for this case. When the jump position was on the E slope, it was, however, lowered by roughly 13–14% with an increase in the  $S'$  value.

The hydraulic jump position in Case EDV<sub>70</sub> remained on the E slope and independent on  $S'$  and  $h'_c$ . When  $V$ 's position was changed, the  $F'_D$  value remained rather constant. The parameter value remained nearly constant for a given  $S'$  value while  $h'_c$  changed. However, when  $h'_c > 0.38$  with  $S'_1$ , it increased by 20%. For this lower porosity of  $V$ , increasing the  $S'$  value decreased  $v$  and the amount of  $F'_D$  from 12 to 20%. Therefore, when the porosity of the vegetation was very low, the increasing length of the open space effectively reduced the dynamic force of the flow.

The result showed that the hydraulic jump type and  $L'_j$  significantly influenced  $F'_D$ . When the open space between E and  $V$  was expanded, a Type-B jump was created, with a very low  $\Phi_1$  of  $V$ , the flow become constant, the surface undulation downstream of the jump decreased, and the tail-water depth in front of  $V$  grew, which contributed to lowering the  $v$ . As a result, the  $F'_D$  decreased to the minimum in Case EDV<sub>70</sub>. Therefore, it was

found that increasing the length of open space effectively reduced the dynamic force of the flow when the porosity of the vegetation was very low.

A crucial factor affecting the structures downstream of the mitigation system is the fluid force index behind the vegetation [13,18,20]. According to recent studies, multiple defense structures have the ability to reduce flow energy both downstream and within the defense structure [20,24,37]. The vulnerability assessment from the 2011 post-tsunami survey and simulation found that the buildings were less prone to damage, which were shielded by steel, masonry, or wood structures [38]. The buildings were adversely affected by both the inundating tsunami depth and the hydrodynamic force. Furthermore, the washed away debris born from the collapsed building or seawalls accelerated the likelihood of structural damage due to its higher momentum force [38,39]. Thus, to reduce the probability of damage of buildings, trees, or other structures behind the mitigation system, however, the fluid force index must be reduced by compound mitigation structures. It was observed that the percentage reduction in  $\Delta FI$  increased as  $h'_c$  rose for all values of  $S'$  in all experimental scenarios. In Cases  $ESV_{98}$  and  $EDV_{88}$ , the reduction amount decreased marginally as the  $S'$  value increased for a given value of  $h'_c$ . Previous studies also found that the  $FI$  was reduced with the increasing  $Fr$  in cases where a single layer of emergent vegetation was employed. However, the pattern was the opposite in Cases  $EDV_{83}$  and  $EDV_{70}$ . When  $h'_c > 0.38$ , it was discovered that the  $\Delta FI$  was reduced by roughly 1–4% as the  $\Phi_I$  decreased. On the other hand, when  $h'_c \leq 0.38$ , it grew by 2–9% while decreasing the  $\Phi_I$ . The reduction in  $\Delta FI(\%)$  was higher in Case  $EDV_{98}$  even though the jump was very near to or inside the  $V$ . Figure 3a makes it evident that there was significant air entrainment via the jump when the vegetation porosity was very low because the jump places were extremely close to  $V$ . Air entrainment through the vegetation increased the water depth and reduced the velocity behind the vegetation, and, due to this, the energy was further reduced downstream [37]. Therefore, under these conditions, air entrainment may help lower the force index due to lowering the velocity. Air entrainment through the vegetation was not detected when the jump position shifted upward, and the  $\Delta FI(\%)$  dropped as the  $S'$  value increased. In the remaining experimental circumstances, the value marginally increased as  $S'$  increased at the time that the Type-B jump developed and somewhat dropped as  $S'$  increased at the time that the Type-B jump changed into either Type-C or Type-A. The porosity of  $V$  was minimum in Case  $EDV_{70}$ , and a Type-B jump was formed regardless of  $h'_c$  and  $S'$ . In relation to  $h'_c$  and  $S'$ , the  $\Delta FI$  grew linearly, and, overall, the reduction in  $\Delta FI$  was between 1% and 4% less than in the other situations.

In supercritical flow conditions, the largest drop in the  $FI$  in the downstream of vegetation was determined to be 16.7%, and this reduction increased with increasing vegetation density downstream of the vegetation [20]. The highest reduction was observed to be almost 80% against a supercritical flow in a complex mitigation system comprising an embankment, 40 rows of vegetation, and a moat [13]. This study used a finite length of both single and double-layer vegetation behind the  $E$  and discovered that, when the  $h'_c$  grew in double-layer vegetation scenarios, the  $FI$  increased as well. The maximum reduction was found to be about 34% and 29–33% in single-layer and double-layer vegetation cases, respectively (Figure 8). The reduction amount was marginally diminished while the vegetation's porosity  $\Phi_I$  was decreased. However, Case  $EDV_{70}$  was shown to be effective in this experiment, considering the decrease in  $F'_D$  and  $\Delta FI$  in front of and behind the vegetation, respectively.

## 5. Conclusions

This study was conducted to find an optimal method for tsunami mitigation by varying the open gap between embankment ( $E$ ) and vegetation ( $V$ ) to understand its effects

within and behind the mitigation system. It was discovered that, when V is positioned downward of E, an upstream hydraulic jump forms, reducing the force of the overtopping flow. When the distance between the E and V models is minimal ( $S_1$ ) and a single layer of vegetation of higher porosity ( $\Phi_1 = 98\%$ ) is used, there is a possibility of the destruction of trees by erosion as the jump occurs within or very close to the vegetation model. On the contrary, the jump shifts upstream when the distance is increased ( $S_2$  and  $S_3$ ). If the  $\Phi_1$  value decreases, the jump position shifts upstream of vegetation, and a Type-B jump occurs even if the  $S_i$  is increased. For the lowest porosity,  $\Phi_1 = 70\%$  with the largest distance  $S_3$ , a Type-B jump was noted for the considered values of  $h'_c$  in this study. It was found that a hydraulic jump was formed, the relative jump length was reduced, and the tail-water depth was sufficient when the value of  $S_i$  was increased. As a result, the water surface level in front of the vegetation becomes almost steady. These were found in Type-B jumps with the maximum distance between E and V. Thus, by controlling the position of the hydraulic jump and its length, scouring around the V and E could be reduced.

In addition, when the jump is fully developed within the attenuation system, the dynamic fluid force ( $F_D$ ) in front of the vegetation is reduced by reducing the velocity. The parameter value is found to be highest because of the higher  $v$  when the jump position is close to the V and lowest as  $v$  lowered when jump location is far upstream and the jump length is shorter.

This study discovered a strong correlation between the hydraulic jump type and the lowering of the  $FI$ . It was slightly reduced when the vegetation's porosity ( $\Phi_1$ ) decreased, and the length of open space ( $S$ ) increased. The maximum reduction was 34% in Case  $ESV_{98}$ , while it was 29% in Case  $EDV_{70}$ . However, Case  $EDV_{70}$  is effective for both tasks when considering the force reduction both in front of V and downstream, which leads not only to downstream safety but vegetation stability as well.

Therefore, in addition to reducing the flow force, considering the resilience of the embankment and vegetation, the porosity of the vegetation should be reduced as much as possible using a submerged layer of vegetation or cylindrical resistance obstacles, and the open space between them should be sufficient. The porosity of vegetation should be moderate if space is limited.

**Author Contributions:** A.H.M.R.; conceptualization, preparing the experimental model, experimental setup, data curation, formal analysis, methodology, visualization, original draft preparation, and review and editing. N.T.; conceptualization, supervision, review and editing, investigation, and funding acquisition. M.A.R.; data curation, visualization, and review and editing. All authors have read and agreed to the published version of the manuscript.

**Funding:** This research received no external funding.

**Data Availability Statement:** Data are contained within this article.

**Acknowledgments:** The authors A H M Rashedunnabi and Md Abedur Rahman acknowledge the support provided by the scholarships from the Japanese Ministry of Education, Culture, Sports, Science, and Technology (MEXT).

**Conflicts of Interest:** Author Md Abedur Rahman was employed by the company Maeda Corporation. The remaining authors declare that the research was conducted in the absence of any commercial or financial relationships that could be construed as a potential conflict of interest.

## Nomenclature

$C_d$	Coefficient of drag for tree
$D$	Diameter of the cylinder used for tree model (m)
$D_{SL}$	Center-to-center distance between the neighboring cylinders in the submerged layer
$D_{EL}$	Center-to-center distance between the neighboring cylinders in the emergent layer (m)
$D_j$	Distance of the hydraulic jump from the vegetation (m)
DV	Double-layer vegetation
E	Embankment
$E_H$	Embankment's height
EL	Emergent layer
$F_D$	Dynamic fluid force (N/m <sup>2</sup> )
$FI$	Fluid force index (m <sup>3</sup> /s <sup>2</sup> )
$Fr$	Froude number
$g$	Acceleration due to gravity (m/s <sup>2</sup> )
$G_{SL}$	Gap between the neighboring cylinders in the submerged layer (m)
$G_{EL}$	Gap between the neighboring cylinders in the emergent layer (m)
$h$	Water depth (m)
$h_c$	Critical overflow depth on the embankment crest (m)
$h_t$	Tail-water depth of the hydraulic jump in front of the vegetation (m)
$h_1$	Water depth in the submerged layer (m)
$h_2$	Water depth in the emergent layer (m)
$L_j$	Length of the hydraulic jump (m)
$n_{t1}$	Number of trees in the submerged layer
$n_{t2}$	Number of trees in the emergent layer
$S$	Distance (open space) between the embankment and vegetation (m)
SV	Single-layer vegetation
V	Vegetation
$V_W$	Vegetation's width
$v$	Velocity (m/s)
$\Phi$	Porosity of the vegetation
$\rho$	Density of water (kg/m <sup>3</sup> )

## References

- Okumura, N.; Jonkman, S.N.; Esteban, M.; Hofland, B.; Shibayama, T. A Method for Tsunami Risk Assessment: A Case Study for Kamakura, Japan. *Nat. Hazards* **2017**, *88*, 1451–1472. [[CrossRef](#)]
- Mori, N.; Takahashi, T.; 2011 Tohoku Earthquake Tsunami Joint Survey Group. Nationwide Post Event Survey and Analysis of the 2011 Tohoku Earthquake Tsunami. *Coast. Eng. J.* **2012**, *54*, 1250001-1–1250001-27. [[CrossRef](#)]
- Suppasri, A.; Shuto, N.; Imamura, F.; Koshimura, S.; Mas, E.; Yalciner, A.C. Lessons Learned from the 2011 Great East Japan Tsunami: Performance of Tsunami Countermeasures, Coastal Buildings, and Tsunami Evacuation in Japan. *Pure Appl. Geophys.* **2013**, *170*, 993–1018. [[CrossRef](#)]
- Mikami, T.; Shibayama, T.; Esteban, M.; Matsumaru, R. Field Survey of the 2011 Tohoku Earthquake and Tsunami in Miyagi and Fukushima Prefectures. *Coast. Eng. J.* **2012**, *54*, 1250011-1–1250011-26. [[CrossRef](#)]
- Jayarathne, M.P.R.; Premaratne, B.; Adewale, A.; Mikami, T.; Matsuba, S.; Shibayama, T.; Esteban, M.; Nistor, I. Failure Mechanisms and Local Scour at Coastal Structures Induced by Tsunami. *Coast. Eng. J.* **2016**, *58*, 1640017. [[CrossRef](#)]
- Tanimoto, R.; Tokida, K.; Kitagawa, H.; Araki, S. Investigation on Resistance of Earth Bank and Reduction by Dug Pool against Tsunami. *Jpn. Soc. Civ. Eng. Ser. B2 (Coast. Eng.)* **2011**, *68*, 316–320. [[CrossRef](#)]
- Temmerman, S.; Meire, P.; Bouma, T.J.; Herman, P.M.J.; Ysebaert, T.; De Vriend, H.J. Ecosystem-Based Coastal Defence in the Face of Global Change. *Nature* **2013**, *504*, 79–83. [[CrossRef](#)] [[PubMed](#)]
- Suppasri, A.; Latcharote, P.; Bricker, J.D.; Leelawat, N.; Hayashi, A.; Yamashita, K.; Makinoshima, F.; Roeber, V.; Imamura, F. Improvement of Tsunami Countermeasures Based on Lessons from the 2011 Great East Japan Earthquake and Tsunami—Situation After Five Years. *Coast. Eng. J.* **2016**, *58*, 1640011-1–1640011-30. [[CrossRef](#)]
- Strusińska-Correia, A. Tsunami Mitigation in Japan after the 2011 Tōhoku Tsunami. *Int. J. Disaster Risk Reduct.* **2017**, *22*, 397–411. [[CrossRef](#)]

10. Usman, F.; Murakami, K.; Kurniawan, E.B. Study on Reducing Tsunami Inundation Energy by the Modification of Topography Based on Local Wisdom. *Procedia Environ. Sci.* **2014**, *20*, 642–650. [[CrossRef](#)]
11. Tanaka, N.; Igarashi, Y. Multiple Defense for Tsunami Inundation by Two Embankment System and Prevention of Oscillation by Trees on Embankment. In Proceedings of the 20th Congress of IAHR APD Congress, Colombo, Sri Lanka, 29–30 August 2016; pp. 28–31.
12. Rahman, M.M.; Schaab, C.; Nakaza, E. Experimental and Numerical Modeling of Tsunami Mitigation by Canals. *J. Waterw. Port Coast. Ocean. Eng.* **2016**, *143*, 04016012-1–04016012-11. [[CrossRef](#)]
13. Zaha, T.; Tanaka, N.; Kimiwada, Y. Flume Experiments on Optimal Arrangement of Hybrid Defense System Comprising an Embankment, Moat, and Emergent Vegetation to Mitigate Inundating Tsunami Current. *Ocean. Eng.* **2019**, *173*, 45–57. [[CrossRef](#)]
14. Rashedunnabi, A.H.M.; Tanaka, N. Energy Reduction of a Tsunami Current through a Hybrid Defense System Comprising a Sea Embankment Followed by a Coastal Forest. *Geosciences* **2019**, *9*, 247. [[CrossRef](#)]
15. Tsujimoto, G.; Mineura, R.; Yamada, F.; Kakinoki, T.; Uno, K. Scouring Mechanism Behind Seawall From Tsunami Overflow and Optimum Conditions To Reduce Tsunami Energy With an Artificial Trench. *Coastal Eng. Proc.* **2014**, *1*, 38. [[CrossRef](#)]
16. Rahman, M.A.; Tanaka, N.; Rehemani, N. Experimental Study on Reduction of Scouring and Tsunami Energy through a Defense System Consisting a Seaward Embankment Followed by Vertically Double Layered Vegetation. *Ocean. Eng.* **2021**, *234*, 108816. [[CrossRef](#)]
17. Bricker, J.D.; Francis, M.; Nakayama, A. Scour Depths near Coastal Structures Due to the 2011 Tohoku Tsunami. *J. Hydraul. Res.* **2012**, *50*, 637–641. [[CrossRef](#)]
18. Tanaka, N.; Onai, A. Mitigation of Destructive Fluid Force on Buildings Due to Trapping of Floating Debris by Coastal Forest during the Great East Japan Tsunami. *Landsc. Ecol. Eng.* **2017**, *13*, 131–144. [[CrossRef](#)]
19. Rahman, M.A.; Tanaka, N. Countermeasure against Local Scouring and Tsunami Damage by Landward Forests behind a Coastal Embankment. *Appl. Ocean. Res.* **2022**, *120*, 103070. [[CrossRef](#)]
20. Murtaza, N.; Pasha, G.A.; Tanaka, N.; Ghani, U.; Anjum, N.; Iqbal, K. Analysis of Hydraulic Jump and Energy Dissipation in Flow Through Emergent Vegetation Under Varying Froude Numbers. *Iran. J. Sci. Technol.-Trans. Civ. Eng.* **2024**. [[CrossRef](#)]
21. Foytong, P.; Ruangrassamee, A.; Shoji, G.; Hiraki, Y.; Ezura, Y. Analysis of Tsunami Flow Velocities during the March 2011 Tohoku, Japan, Tsunami. *Earthq. Spectra* **2013**, *29*, S161–S181. [[CrossRef](#)]
22. Nandasena, N.A.K.; Tanaka, N.; Sasaki, Y.; Osada, M. Boulder Transport by the 2011 Great East Japan Tsunami: Comprehensive Field Observations and Whither Model Predictions? *Mar. Geol.* **2013**, *346*, 292–309. [[CrossRef](#)]
23. Pasha, G.A.; Tanaka, N. Undular Hydraulic Jump Formation and Energy Loss in a Flow through Emergent Vegetation of Varying Thickness and Density. *Ocean. Eng.* **2017**, *141*, 308–325. [[CrossRef](#)]
24. Rahman, M.A.; Tanaka, N.; Rashedunnabi, A.H.M. Flume Experiments on Flow Analysis and Energy Reduction through a Compound Tsunami Mitigation System with a Seaward Embankment and Landward Vegetation over a Mound. *Geosciences* **2021**, *11*, 90. [[CrossRef](#)]
25. Hager, W.H. B-Jump in Sloping Channel. *J. Hydraul. Res.* **1988**, *26*, 539–558. [[CrossRef](#)]
26. Kawagoshi, N.; Hager, W.H. B-Jump in Sloping Channel, II. *J. Hydraul. Res.* **1990**, *28*, 461–480. [[CrossRef](#)]
27. Chanson, H. *The Hydraulics of Open Channel Flow: An Introduction: Basic Principles, Sediment Motion, Hydraulic Modelling, Design of Hydraulic Structures*, 2nd ed.; Butterworth-Heinemann: Oxford, UK, 2004; ISBN 9780080472973 | 0750659785 | 9780750659789.
28. Wei, C.Y.; Lindell, J.E. Hydraulic Design of Stilling Basins and Energy Dissipators. In *Hydraulic Design Handbook*; McGraw-Hill: New York, NY, USA, 2004; pp. 1–55.
29. Pakoksung, K.; Suppasri, A.; Imamura, F. Systematic Evaluation of Different Infrastructure Systems for Tsunami Defense in Sendai City. *Geosciences* **2018**, *8*, 173. [[CrossRef](#)]
30. Ohtsu, I.; Yasuda, Y. Hydraulic Jump in Sloping Channels. *J. Hydraul. Eng.* **1991**, *117*, 905–921. [[CrossRef](#)]
31. Pasha, G.A.; Tanaka, N. Characteristics of a Hydraulic Jump Formed on Upstream Vegetation of Varying Density and Thickness. *J. Earthq. Tsunami* **2020**, *14*, 2050012. [[CrossRef](#)]
32. Ohtsu, I.; Yasuda, Y.; Takahashi, M. Flow Characteristics of Skimming Flows in Stepped Channels. *J. Hydraul. Eng.* **2004**, *130*, 860–869. [[CrossRef](#)]
33. Matsuba, S.; Mikami, T.; Jayaratne, R.; Shibayama, T.; Esteban, M. Analysis of Tsunami Behavior and the Effect of Coastal Forest in Reducing Tsunami Force Around the Coastal Dikes. *Coast. Eng. Proc.* **2014**, *1*, 37. [[CrossRef](#)]
34. Rahman, M.A.; Tanaka, N.; Anjum, N. Damming Effects of Tsunami-Borne Washed-out Trees in Reducing Local Scouring and Tsunami Energy behind a Coastal Embankment. *Appl. Ocean. Res.* **2022**, *126*, 103260. [[CrossRef](#)]
35. Dissanayaka, K.D.C.R.; Tanaka, N. Comparison of the Flow around Circular and Rectangular Emergent Cylinders with Subcritical and Supercritical Conditions. *Fluids* **2023**, *8*, 124. [[CrossRef](#)]
36. Tanaka, N.; Sasaki, Y.; Mowjood, M.I.M.; Jinadasa, K.B.S.N.; Homchuen, S. Coastal Vegetation Structures and Their Functions in Tsunami Protection: Experience of the Recent Indian Ocean Tsunami. *Landsc. Ecol. Eng.* **2007**, *3*, 33–45. [[CrossRef](#)]

37. Rashedunnabi, A.H.M.; Tanaka, N. Effectiveness of Double-Layer Rigid Vegetation in Reducing the Velocity and Fluid Force of a Tsunami Inundation behind the Vegetation. *Ocean. Eng.* **2020**, *201*, 107142–107154. [[CrossRef](#)]
38. Scorzini, A.R.; Di Bacco, M.; Sugawara, D.; Suppasri, A. Machine Learning and Hydrodynamic Proxies for Enhanced Rapid Tsunami Vulnerability Assessment. *Commun. Earth Environ.* **2024**, *5*, 301. [[CrossRef](#)]
39. Di Bacco, M.; Rotello, P.; Suppasri, A.; Scorzini, A.R. Leveraging Data Driven Approaches for Enhanced Tsunami Damage Modelling: Insights from the 2011 Great East Japan Event. *Environ. Model. Softw.* **2023**, *160*, 105604. [[CrossRef](#)]

**Disclaimer/Publisher’s Note:** The statements, opinions and data contained in all publications are solely those of the individual author(s) and contributor(s) and not of MDPI and/or the editor(s). MDPI and/or the editor(s) disclaim responsibility for any injury to people or property resulting from any ideas, methods, instructions or products referred to in the content.